Original Article

Whole brain atlas-based diffusion kurtosis imaging parameters for the evaluation of multiple cognitive-related brain microstructure injuries after radiotherapy in lung cancer patients with brain metastasis

Xuyun Xie[1#], Min Feng[2#], Yi Rong[3], Jiamiao Hu[1], Weiwen Zhou[1], Ying Li[4], Hailong Liao[1], Liming Shi[1], Hongjian He[2], Qiqi Tong[5], Xiaonan Sun[1]

[1]Department of Radiation Oncology, Sir Run Run Shaw Hospital, School of Medicine, Zhejiang University, Hangzhou, China; [2]Center for Brain Imaging Science and Technology, College of Biomedical Engineering and Instrument Science, Zhejiang University, Hangzhou, China; [3]Department of Radiation Oncology, Mayo Clinic Arizona, Phoenix, AZ, USA; [4]Department of Nursing, Sir Run Run Shaw Hospital, School of Medicine, Zhejiang University, Hangzhou, China; [5]Research Center for Healthcare Data Science, Zhejiang Lab, Hangzhou, China

Contributions: (I) Conception and design: X Xie, M Feng, Q Tong; (II) Administrative support: Q Tong, H He, X Sun; (III) Provision of study materials or patients: X Xie, J Hu, W Zhou, L Shi; (IV) Collection and assembly of data: X Xie, J Hu, W Zhou, Y Li, H Liao, L Shi; (V) Data analysis and interpretation: X Xie, M Feng, Q Tong; (VI) Manuscript writing: All authors; (VII) Final approval of manuscript: All authors.

[#]These authors contributed equally to this work.

Correspondence to: Dr. Xiaonan Sun, MD, PhD. Department of Radiation Oncology, Sir Run Run Shaw Hospital, School of Medicine, Zhejiang University, 3 Qingchun East Road, Hangzhou 310016, China. Email: sunxiaonan@zju.edu.cn; Prof. Hongjian He, PhD. Center for Brain Imaging Science and Technology, College of Biomedical Engineering and Instrument Science, Zhejiang University, #38 Zheda Road, Hangzhou 310013, China. Email: hhezju@zju.edu.cn; Qiqi Tong, PhD. Research Center for Healthcare Data Science, Zhejiang Lab Nanhu Headquarters, Kechuang Avenue, Zhongtai Sub-District, Yuhang District, Hangzhou 311121, China. Email: tongqq@zhejianglab.com.

Background: Whole brain radiation therapy (WBRT) can cause cognitive dysfunctions in lung cancer patients with brain metastasis (BM). Diffusion kurtosis imaging (DKI) can detect brain microstructural alterations sensitivly. We aimed to identify the potential of DKI parameters for early radiation-induced brain injury and investigate the association between microstructure changes and neurocognitive function (NCF) decline.

Methods: Lung cancer patients with BM (n=35) who underwent WBRT in a single center in Zhejiang, China, were consecutively and prospectively enrolled between June 24th, 2020 and December 22nd, 2021, and the median follow-up time was 6.0 months (3.6–6.6 months). DKI and T1-weighted (T1W) MRI scans were acquired prior to and following WBRT. Diffusivity-based (mean diffusivity, MD; fractional anisotropy, FA) and kurtosis-based (mean kurtosis, MK; axial kurtosis, AK) parameters were calculated within the automated anatomical labeling (AAL) atlas-based regions. Reliable change indices practice effects (RCI-PE) scores of the Mini-Mental State Examination (MMSE) were calculated to determine significant neurocognitive decline by a one-sample *t*-test from baseline to 2–6 months post-WBRT. To assess the subacute induced effects within the whole brain, percentage changes of DKI parameters were evaluated at 170 atlas-based regions by a one-sample *t*-test. Linear regression analyses were used to evaluate the association between DKI parameter changes and RCI-PE scores.

Results: Finally, the study included 19 patients in the longitudinal follow-up. RCI-PE scores declined at 2–6 months post-WBRT (mean RCI-PE =–0.842, 95% CI, –0.376 to –1.310; P=0.002). With the atlas-based analysis of subacute effects after post-WBRT, a total of 28 regions changed in at least one diffusion parameter, revealing region-wise microstructural alterations in the brain. Significant correlations of at least

one diffusion parameters with RCI-PEs were observed in 9 regions, such as the right orbital part of the inferior frontal gyrus [right IFGorb, r(AK) =0.47, P=0.03] and left middle temporal gyrus [left MTG, r(MK) =–0.49, P=0.03].

Conclusions: DKI parameters can be used to detect early microstructure changes and represent important imaging predictors for cognitive decline. The reported 9 regions are more particularly vulnerable to neurocognitive radiation-induced impairment for lung cancer patients with BM, representing potential dose-avoidance targets for cognitive function preservation.

Keywords: Brain metastasis (BM); lung cancer; radiation-induced cognitive injury; diffusion kurtosis imaging (DKI); brain microstructure

Submitted Dec 11, 2022. Accepted for publication Jun 06, 2023. Published online Jun 25, 2023.
doi: 10.21037/qims-22-1376
View this article at: https://dx.doi.org/10.21037/qims-22-1376

Introduction

Lung cancer is one of the most common malignant tumors worldwide, with an incidence rate of 20–40% for brain metastasis (BM), and the median survival time of untreated patients is often less than 3 months (1). The current mainstream treatments for BM include whole-brain radiation therapy (WBRT) and stereotactic radiosurgery (SRS), with unavoidable radiation doses spilling into the normal brain (2). Radiation-induced side effects may cause long-term cognitive impairment, such as memory loss, intelligence retardation, reaction bluntness, language and executive dysfunction (3,4), which deteriorates patients' quality of life (QOL). Until the emergence of more advanced targeted therapy or immunotherapy for prolonged survival and reduced brain injury (5,6), patients with BM will still suffer from brain injury post-radiotherapy. A personalized radiotherapy strategy for brain metastases that can protect cognitive function as much as possible under the premise of ensuring curative effects, deserves attention.

According to recent research, radiation-induced brain injury is characterized by vascular abnormalities, demyelination, neuroinflammation, and ultimately white and gray matter necrosis (7). This involves multiple regions of the brain rather than the hippocampus alone. Non-hippocampus regions, such as the medial temporal lobe (8), left-sided perisylvian white matter (9), and bilateral cingulate angular bundle (CAB) fibers (10), have been found to be associated with neurocognitive function (NCF) decline in patients with primary brain tumors and nasopharyngeal carcinoma receiving radiotherapy (RT). The present anatomical avoidance strategies of radiotherapy for brain metastases are mostly related to the hippocampus (11,12). NRG CC001, a phase III trial of WBRT + memantine (WBRT + M) with or without hippocampal avoidance (HA), reported a lower standardized NCF failure rate in the HA-WBRT group than in the WBRT without HA group (58% *vs.* 69.1%). In this study, more than half of patients still had NCF failure despite avoiding the hippocampus. Thus, leading us to wonder if other cognitively related areas outside the hippocampus have not been adequately protected. SRS represents an important strategy to improve local control and to reduce cognitive decline (13). However, most studies on SRS focus on the number and volume of tumors and have not paid much attention to the setting of organs at risk (OAR) and threshold doses. Brain microstructures (14), with their unique cell types, anatomical structures, and immune environment, may provide new ways to protect cognitive function.

Two main challenges exist in current detection methods in terms of clinically observed correlations between whole brain microstructure changes and cognitive function. First, due to the special neural function and anatomical structure of the brain, it is difficult to observe these changes by pathological tissue biopsy or peripheral blood tests. Diffusion weighted (DW) magnetic resonance imaging (MRI) is a widely used and powerful technique for evaluating microstructural integrity and alterations by its model-driven parameters (15). Specifically, diffusion tensor imaging (DTI) assumes a Gaussian distribution for water molecule displacement and has been found to be a viable biomarker for identifying RT-associated white matter microstructural injury (16). However, the brain microstructural components in the brain, such as cell

membranes and intracellular and extracellular spaces, make the water distribution behave in a non-Gaussian manner. Diffusion kurtosis imaging (DKI) is more sensitive to evaluate such microstructural pathological changes in non-Gaussian water distribution (17). Application has shown that DKI can detect RT-induced changes in the temporal lobe (18,19). Second, the brain parenchyma contains many cell types, such as astrocytes, microglia, oligodendrocytes, and neurons, so radiosensitivity varies greatly across different regions (14). There is usually a large radiation dose difference when using SRS for BM and primary brain tumors, introducing dose-dependent variations, which makes WBRT a better observation model due to its higher homogeneity in dose distributions.

This prospective study of patients with brain metastases receiving WBRT was designed to investigate the association between structural and microstructural changes in the whole brain and post-RT decline in the Mini-Mental State Examination (MMSE) using DKI. We aim to identify regions that may be associated with NCF tests for dose-avoidance to protect cognitive functions, while not reducing the prescribed radiation dose of brain metastases. We present this article in accordance with the STROBE reporting checklist (available at https://qims.amegroups.com/article/view/10.21037/qims-22-1376/rc).

Methods

Study design and participants

The study was conducted in accordance with the Declaration of Helsinki (as revised in 2013). The study was approved by the ethics committee of Sir Run Run Shaw Hospital (No. 20200416001) and informed consent was taken from all individual participants. This study prospectively enrolled 35 patients with BM from lung cancer, who received WBRT at our institution from June 24th, 2020, to December 22nd, 2021. Specifically, T1 weighted (T1W) and DW scans were obtained within 0–7 days before and after radiotherapy for each patient. The association between early changes in DKI and MMSE scores was evaluated both before and after WBRT. Telephone contact and visits were undertaken to record the patients' information, and the follow-up procedures were the same for all participants. The follow-up period was defined as the time from the first date of WBRT to April 13th, 2022.

The inclusion criteria were as follows: completed neurocognitive assessments, age ≥18 years, Karnofsky performance status (KPS) ≥70 and expected survival time >6 months [Gustave Roussy Immune (GRIm) Score <1 (20)]. The exclusion criteria were patients who received prior WBRT or had meningeal metastasis.

Radiotherapy protocol

Radiation therapy planning computed tomography (CT) with 2-mm slice thickness was performed with the patient in thermoplastic mask immobilization. Whole brain planning target volume (PTV) was defined as the whole-brain parenchyma with a 3-mm margin. The eyes, lenses, optic nerves, optic chiasm, inner ears and brainstem were additionally defined as OAR. Contouring and treatment planning were developed using a three-dimensional radiation therapy planning system (Eclipse V11.0; Varian Medical Systems, Palo Alto, CA, USA). The prescribed dose was 25 Gy for prophylactic cranial irradiation (PCI), and 30 Gy for patients with BM, all of which were delivered in 10 fractions.

Neurocognitive assessment

MMSE was used to assess NCF prior to radiotherapy, 1 month to radiotherapy and every 3 months after radiotherapy in patients, including five cognitive domains: orientation, memory, the capability of attention and calculation, delayed recall and language. The evaluation time is approximately 10 minutes, administered by professional psychologists. Because repeated tests may produce errors due to practice effects, this article uses reliable change indices (RCI-PE) scores instead of MMSE scores (21).

Imaging acquisition and processing

MRI images were acquired in a Siemens 3T scanner (MAGNETOM Skyra, Siemens Healthcare, Erlangen, Germany) equipped with a 64-channel RF head coil. The sequences obtained included a 3-dimensional T1W magnetization-prepared rapid acquisition with gradient echo (MPRAGE) sequence [repetition time (TR) =2,200 ms; echo time (TE) =2.48 ms; inversion time =900 ms; flip angel =8 degrees; field of view (FOV) =230 mm; matrix =256×256; resolution =0.9 mm × 0.9 mm; slice thickness =1 mm; 176 slices] and diffusion-weighted imaging (DWI) using a single-shot diffusion echo-planar imaging (EPI) sequence (TR =10,400 ms; TE =96 ms, FOV =220 mm; matrix =110×110;

resolution =2 mm × 2 mm; slice thickness =2.0 mm; 70 slices), with b=0, 1,000, 2,000 s/mm^2 applied in 1, 30, and 30 unique gradient encoding directions for each b-value, respectively. Three additional b=0 volumes with reversed-phase encoded polarity were acquired for nonlinear B0 distortion correction.

The preprocessing steps were implemented in the FMRIB Software Library (FSL, University of Oxford, UK). All T1W images were first sublected to bias correction and skull extraction using the FSL_ANAT function and parcellated into 170 regions of interest (ROIs) based on the automated anatomical labeling (AAL) atlas (22), a widely used cortical parcellation map, after nonlinear registration from standard space to each subject's T1W space. For each DWI scan, we corrected eddy current distortion, head motion, and EPI distortion correction using the EDDYCORRECT function. Non-brain tissue from the average b0 images was removed using the Brain Extraction Toolbox (BET). A b0 signal correction (23) and constrained weighted linear least square fitting (24) were employed to derive both tensor-based parameters mean diffusivity (MD) and fractional anisotropy (FA) and kurtosis-based parameters mean kurtosis (MK) and axial kurtosis (AK). Next, these diffusion parameters were coregistered to individual high-resolution baseline T1W images and segmented into corresponding ROIs through the registered AAL atlas.

Images were meticulously inspected for registration or segmentation errors. We manually created a censoring mask, drawn slice-by-slice, comprising the tumor, surgical bed, edema, and other radiographic abnormalities separately for each patient and verified by two imaging experts. All voxels in the censoring mask were eliminated from the analysis to avoid confounding from tumor and edema-related effects.

Study size

Use PASS 15 software (Power Analysis and Sample Size) to estimate the sample size, group K=1, according to the significance level of the bilateral test α=0.05, Power =0.9. In this study, through preliminary experiments, the calculated standard deviation was 1.65, and the calculated sample size was 32, with a statistical difference. Based on a 20% dropout rate, 32 × (1+0.2)=38 cases are required for each group, and the sample size for this study is estimated to be 38 cases. However, due to the slow progress of enrollment, the study was terminated early in 35 cases.

Statistical analysis

Statistics were performed in SPSS v26 (IBM Corp., Chicago, USA). A one-sample *t*-test was used to determine significant group changes in RCI-PEs from baseline to 2–6 months post-WBRT (H_0 =0). Associations between 2–6 months RCI-PEs and patient characteristics (i.e., gender, age, education level, basic MMSE performance, MMSE time from WBRT, tumor volume percentage, pathology, systemic treatment, prednisone and total dose) were evaluated by Pearson correlations, the independent sample *t*-test and one-way analysis of variance.

Percentage changes in diffusion parameters (MD, FA, MK and AK) were calculated as the difference between pre-WBRT and post-WBRT in a percentage unit. To assess the subacute WBRT effects within the whole brain, the region-specific diffusion parameter changes were evaluated by a one-sample *t*-test (H_0 =0).

$$\Delta M = \frac{M_{\text{post}} - M_{pre}}{M_{pre}} \times 100\% \quad [1]$$

where M is the diffusion metrics measured pre- and post-WBRT. To control for multiple comparisons, a false discovery rate (FDR) of 0.05 was performed using the Benjamini-Hochberg method. Linear regression analyses were used to evaluate the association between diffusion changes (ΔM) and RCI-PE scores, while controlling for age, gender and any significant univariate predictors.

Results

Patient characteristics and their associations with RCI-PE scores

Upon completion of the prospective trial, 19 patients (13 males and 6 females, median age 62 years) with complete imaging and cognitive data were selected for further data analysis, with the selection process shown in *Figure 1*. The pathology type had a slight majority of small cell carcinoma (58%). Nearly half of the patients had received education above junior high school. The primary tumor was stable in 11 cases and unstable in 7 cases, and the remaining tumor was untreated due to the discovery of BM at the same time as the primary tumor. Three out of 19 did not use prednisone during radiotherapy. The majority of patients had undergone systemic therapy after WBRT, and six patients did not receive subsequent systematic therapy due to unnecessary treatment, chemotherapy intolerance,

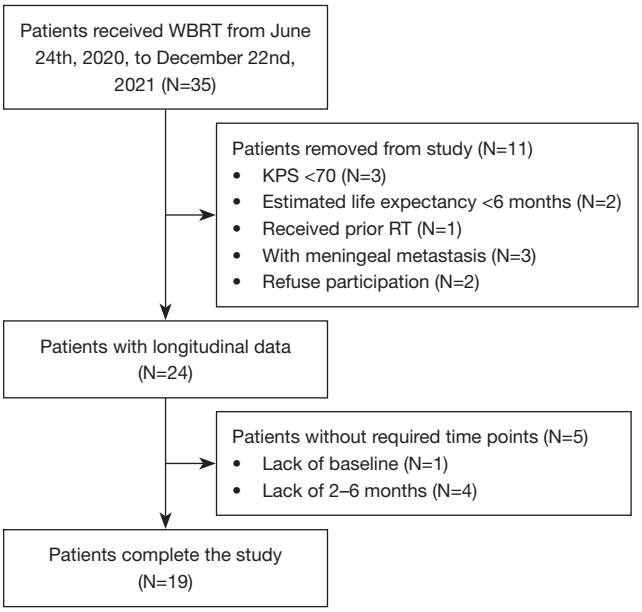

Figure 1 A workflow diagram for cases selection. WBRT, whole brain radiation therapy; KPS, Karnofsky performance status; RT, radiotherapy.

financial reasons, or a shortage of effective treatment at that time. The tumor area was delineated by an experienced radiologist and the volume was automatically calculated by the radiotherapy planning system, ranging from 0.23 to 77.91 cm^3.

A significant group decline from baseline was observed at 2–6 months post-WBRT in RCI-PE scores (mean RCI-PE =−0.842, 95% CI, −0.376 to −1.310; P=0.002). No significant correlations were observed between clinical covariates and RCI-PE scores for MMSE tests (all P>0.05).

The patients' clinical characteristics and analyses of the associations between patient characteristics and RCI-PE scores are shown in *Table 1*.

Table 1 Clinical characteristics of 19 patients who were finally included in this study and their associations with RCI score

Characteristic	Patients, n [%]	P value
Gender		0.81
Male	13 [68]	
Female	6 [32]	
Age (years), median [range]	62 [50–77]	0.24
Education		0.75
Primary school or lower	9 [47]	
Junior high school or higher	10 [53]	
Pathology		0.29
Small cell carcinoma	11 [58]	
Non-small cell carcinoma	8 [42]	
Primary disease control		0.28
Stable	11 [58]	
Progress	7 [37]	
Not yet treated	1 [5]	
Other metastases		0.19
Yes	9 [47]	
No	10 [53]	
Systemic treatment		0.44
Chemotherapy	9 [47]	
Target-treatment	6 [32]	
Immunotherapy	5 [26]	
None	6 [32]	
Tumor volume (cm^3), median [range]	0.23 [0–77.91]	0.35
Prednisone		0.16
Yes	16 [84]	
No	3 [16]	

RCI, reliable change indices.

Subacute WBRT effects: diffusion parameter changes after WBRT

With the atlas-based analysis of subacute effects post-WBRT, a total of 28 ROIs demonstrated significant changes in at least one diffusion parameter from the baseline, revealing region-wise microstructural alterations in the brain. The main clusters of these regions were in the left frontal gyrus (middle, and inferior portions), the left temporal gyrus (superior, middle, and inferior portions). In addition, individual regions that included the fusiform gyrus (FFG), the caudate nucleus had significant changes from baseline post-WBRT. The details regarding the subregions with significant changes and their diffusion responses are summarized in Table S1. MD, FA, MK and AK could detect microstructure alterations in 12, 2, 23 and 23 atlas-based regions respectively. BM patients had significantly decreased DKI-derived kurtosis-based parameters (MK, AK) in 13 atlas-based regions (P≤0.05, FDR-BH corrected) while no significant observation was found in the tensor-based

Table 2 Region of interest analysis of subacute WBRT effect on each parameter: mean percentage change and P values by one-sample *t*-test

Region of interest	MD		FA		MK		AK	
	Percentage change	P value	Percentage change	P value	Percentage change	P value	Percentage change	P value
Frontal gyrus								
Left IFGoperc	1.48 (3.55)	0.12	−0.75 (6.37)	0.62	−1.36 (2.12)	0.02*	−1.58 (2.14)	0.02*
Left IFGtriang	2.36 (4. 09)	0.02*	−1.51 (3.76)	0.10	−1.67 (1.96)	0.004*	−2.16 (2.26)	0.004*
Right IFGorb	4.66 (5.25)	0.004*	−2.47 (5.34)	0.06	−1.39 (2.78)	0.05*	−1.67 (2.50)	0.02*
Right SFGmedial	1.46 (6.01)	0.31	−1.87 (7.10)	0.37	−2.24 (3.13)	0.03*	−2.22 (3.18)	0.01*
Parahippocampal gyrus								
Right PHG	5.10 (9.65)	0.06	−1.63 (6.25)	0.28	−1.21 (1.86)	0.04*	−1.16 (2.96)	0.14
Fusiform gyrus								
Right FFG	4.31 (7.04)	0.02*	0.29 (6.86)	0.86	−1.25 (1.58)	0.01*	−0.99 (3.54)	0.33
Paracentral lobule								
Left PCL	3.81 (11.07)	0.16	−4.06 (6.83)	0.04*	−2.55 (4.94)	0.05*	−2.50 (3.20)	0.01*
Temporal gyrus								
Left MTG	2.57 (4.54)	0.04*	−1.08 (5.84)	0.58	−1.82 (1.99)	0.004*	−1.90 (2.05)	0.004*
Left ITG	2.41 (3.56)	0.01*	0.25(6.09)	0.86	−1.78 (2.15)	0.006*	−2.12 (2.28)	0.004*

Data are shown as mean (SD). *, P values indicate statistical significance (P≤0.05) after corrections for multiple comparisons. WBRT, whole brain radiation therapy; MD, mean diffusivity; FA, fractional anisotropy; MK, mean kurtosis; AK, axial kurtosis; IFGoperc, opercular part of inferior frontal gyrus; IFGtriang, triangular part of inferior frontal gyrus; IFGorb, orbital part of inferior frontal gyrus; SFGmedial, medial orbital part of superior frontal gyrus; PHG, parahippocampal gyrus; FFG, fusiform gyrus; PCL, paracentral lobule; MTG, middle temporal gyrus; ITG, inferior temporal gyrus; SD, standard deviation.

parameters, MD and FA, which suggest that MK and AK might have higher sensitivity than MD and FA in detecting subacute brain microstructural changes after WBRT. *Table 2* lists each parameter's average changes in the 9 identified regions detected from the subsequent atlas-based regions analysis which had a significant association with cognitive function. These representative atlas-based regions in the brain are shown and labeled in *Figure 2*.

Early diffusion parameter changes associated with cognitive-related microstructural injury

Clinical characteristics and cognitive test performance were not significantly correlated (P>0.05). Therefore, only age and gender were included as covariates in the linear regression model. MD, FA, MK and AK within those atlas-based regions with significant changes were investigated as predictors of MMSE changes post-WBRT. Significant correlation of predictors with RCI-PEs were observed in 9 regions, distributed in frontal, parahippocampal, fusiform, temporal gyrus and paracentral lobule (PCL) (*Table 2* and *Figure 2*).

For the frontal gyrus, the following regions significantly associated with RCI-PE scores: the left triangular part of the inferior frontal gyrus [left IFGtriang, r(MD) =0.48, P=0.03], the left opercular part of the inferior frontal gyrus [left IFGoperc, r(MK) =−0.49, P=0.03], the right orbital part of the inferior frontal gyrus [right IFGorb, r(AK) =0.47, P=0.03], and the right medial orbital part of the superior frontal gyrus [right medial orbital part of superior frontal gyrus (SFGmedial), r(MK) =−0.47, P=0.04]. The RCI-PE scores showed a positive correlation with MD percentage changes in the left inferior temporal gyrus [left inferior temporal gyrus (ITG), r(MD) =0.51, P=0.02] and a negative correlation with MK percentage changes in the left middle temporal gyrus [left middle temporal gyrus (MTG), r(MK) =−0.49, P=0.03]. Last, the right FFG [r(MD) =0.57, P=0.01], the left PCL [r(FA) =−0.47, P=0.04] and the right parahippocampal gyrus [right parahippocampal gyrus (PHG), r(MK) =−0.45, P=0.04] were also found to

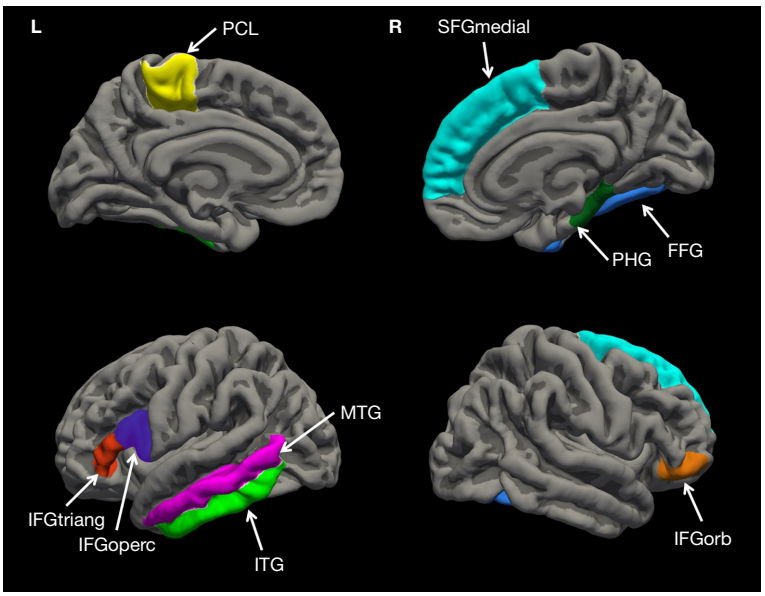

Figure 2 Representative segmentation of 9 regions where significant microstructure changes after WBRT and associated with RCI-PE scores are overlaid on a left and right brain surface from the AAL atlas. The ROIs include left PCL (yellow), left IFGtriang (red), left IFGoperc (dark purple), left MTG (magenta), left ITG (green); right SFGmedial (cyan), right PHG (dark green), right FFG (blue), and right IFGorb (orange). L, left; PCL, paracentral lobule; IFGtriang, triangular part of inferior frontal gyrus; IFGoperc, opercular part of inferior frontal gyrus; MTG, middle temporal gyrus; ITG, inferior temporal gyrus; R, right; SFGmedial, medial orbital part of superior frontal gyrus; PHG, parahippocampal gyrus; FFG, fusiform gyrus; IFGorb, orbital part of inferior frontal gyrus; WBRT, whole brain radiation therapy; RCI-PE, reliable change indices practice effects; AAL, automated anatomical labeling; ROI, regions of interest.

be associated with poorer performance on the MMSE test. *Figure 3* shows the above mentioned corresponding correlations with RCI-PE scores. The diffusion parameters of the remaining atlas-based regions did not show significant correlations with the RCI-PE scores.

Discussion

In this prospective longitudinal investigation of lung cancer patients with BM who underwent WBRT, we found that radiation injury to brain microstructural markers in several regions across the brain was significantly correlated with cognitive decline. DKI-derived kurtosis parameters (MK, AK) and diffusion parameters (MD, FA) were able to describe changes in these areas, including 4 atlas-based regions within the frontal gyrus (IFGoperc, IFGtriang, IFGorb, and SFGmedial), 2 atlas-based regions within the temporal gyrus (ITG and left MTG), and the PHG, FFG and PCL. These findings were expected given that cognitive function is a complex array of functions affected by multiple brain microstructures, fiber bundles, and microenvironments. In addition, we found that radiation damage varies between different regions in the brain even when irradiated with the same dose level.

Approximately 90% of patients who receive WBRT suffer a certain degree of radiation-induced cognitive impairment (2). The human brain has been thought to be radioresistant in the past, and white matter necrosis was recognized as a late side-effect 6 months after irradiation. Recent studies have reported earlier brain injury after radiotherapy, which may be more meaningful than severe cognitive impairment after 6 to 12 months. Three months after WBRT, Rola *et al.* reported impairments in spatial learning and memory associated with neuronal maturation deficits (25). Among 41 patients with supratentorial tumors, cognitive impairment was observed 1.5 months after brain RT and recovery 4.5 months after brain RT (26). Our research detected a significant group decline from baseline to 2–6 months post-WBRT in RCI-PE scores. However, the follow-up of neurological function after 6 to 12 months of this study has not been completed; there are insufficient data to verify whether the injury can be recovered yet.

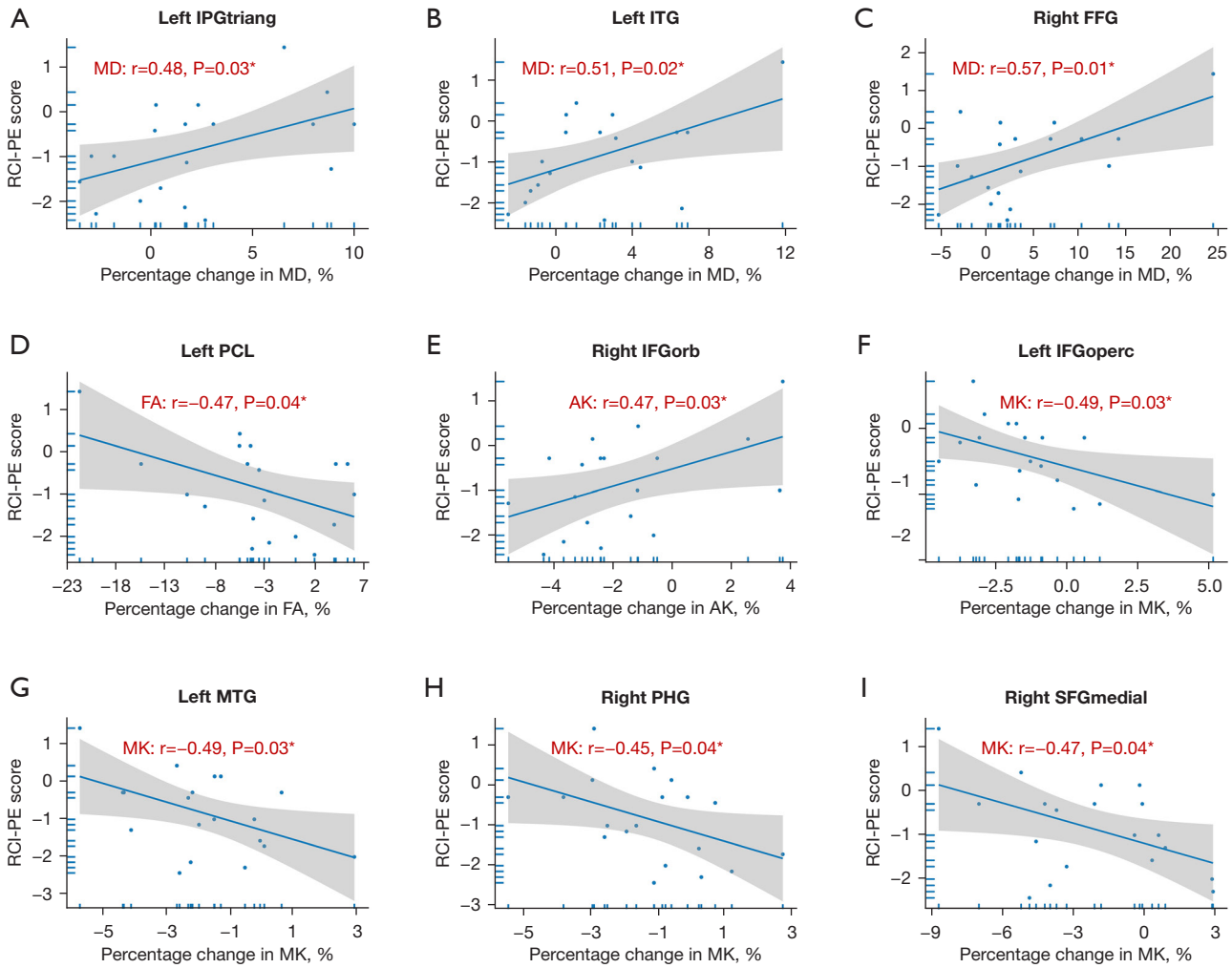

Figure 3 Scatter plots demonstrating correlation between the RCI-PE scores and the percentage changes of diffusion parameter in each region. The regression lines indicate the association between diffusion percentage changes and RCI-PE scores. Age and gender were treated as co-variates for RCI-PE scores feature in the regression models. Only significant correlations between any of the diffusion parameters and RCI-PE scores were marked with the Pearson's correlation coefficient and P value. (A) The RCI-PE scores and the percentage change in MD in left IFGtriang. (B) The RCI-PE scores and the percentage change in MD in left ITG. (C) The RCI-PE scores and the percentage change in MD in right FFG. (D) The RCI-PE scores and the percentage change in FA in left PCL. (E) The RCI-PE scores and the percentage change in AK in right IFGorb. (F) The RCI-PE scores and the percentage change in MK in left IFGoperc. (G) The RCI-PE scores and the percentage change in MK in left MTG. (H) The RCI-PE scores and the percentage change in MK in right PHG. (I) The RCI-PE scores and the percentage change. MK in right SFGmedial. *, significant results (P<0.05). RCI-PE, reliable change indices practice effects; IFGtriang, triangular part of inferior frontal gyrus; MD, mean diffusivity; ITG, inferior temporal gyrus; FFG, fusiform gyrus; PCL, paracentral lobule; FA, fractional anisotropy; IFGorb, orbital part of inferior frontal gyrus; AK, axial kurtosis; IFGoperc, opercular part of inferior frontal gyrus; MK, mean kurtosis; MTG, middle temporal gyrus; PHG, parahippocampal gyrus; SFGmedial, medial orbital part of superior frontal gyrus.

Prior to the 1990s, the pathogenesis of radiation-induced injury was often considered a decrease in the number and volume of neurons and is now believed to be a complex and dynamic interactions and process occurring in multiple cell types within brain microstructures, including neuronal demyelination (27), a chronic inflammatory state (28), abnormal hyperplasia and necrosis of blood vessels (29). These changes in brain microstructural organization are

difficult to observe in time because of the constrains to performing brain tissue biopsy and the existence of the blood brain barrier. The literature reports extensive studies of DTI (30) and DKI (31-33) parameters for brain sub-function regions. Similar to DTI-based biomarkers, these DKI parameters reflect the heterogeneity of the intravoxel diffusion environment and are therefore indicators of microstructural complexity in many diseases (15). To date, there has been no report on the correlation between the performance of DKI parameters and cognitive decline post radiotherapy for brain metastases; thus, the present study starts to satisfy this dire need.

Remarkably, changes in cognitive function after brain radiotherapy are associated with the interplay of multiple structures and thus cannot be simply attributed to single structure or volume changes. In our study, the increase in MK changes in the right SFGmedial, right PHG, right FFG and left MTG had a significant correlation with the decrease in the MMSE RCI-PE. Consistent with previous knowledge, cognitive functions are performed by specialized brain regions, while interneural connections cooperate and coordinate their action. For example, the language center is composed of the IFG, MTG, and superior temporal gyrus (STG), which perform semantic processing (34), syntactic combining (35), and reading skills, respectively. Note that only the middle part of the SFG was associated with the decline in RCI-PE scores in our study, instead of the whole region of the SFG. The same results had also reported that the IFGoperc lies in the motor speech center and that the DL-SFG is related to Parkinson's disease (36) but not the whole region. This leads to the hypothesis that more accurate protection can be achieved by identifying sub-regions of atlas-based regions for brain radiotherapy. Likewise, sub-region changes correlated with more advanced cognitive impairment remain unclear and need to be verified in a study with a longer follow-up.

The prolonged survival time for patients with brain metastases emphasized the importance of preserving cognitive function. We observed statistically significant correlation between the changes in diffusion parameters and cognitive impairment after radiotherapy in the PHG, but not in other parts of the hippocampus. This may be due to the different radio-sensitivity in brain structures. As an important part of the hippocampal circuit, PHG is related to high-level neurological and cognitive activities such as emotion, learning and memory. Hippocampus avoidance has been a main focus of most clinical trials. A glioma RT study showed that regions of adult neurogenesis primarily predict cognition at %v40 (percent of ROI receiving 40 Gy) and %v10 (percent of ROI receiving 10 Gy) for the right hippocampus (37). The existing hippocampal protection strategies limit the maximum dose at 17 Gy (11,12). In our study, however, the entire brain was exposed to more than 25 Gy of radiation, which may affect the assessment of hippocampal changes. It will be necessary to conduct studies with a larger number of patients in the future using more dosing methods.

However, hippocampal-sparing alone may be insufficient to spare cognitive function after brain RT. Schindler *et al.* showed that older rats with cognitive dysfunction after WBRT fail to show a radiation-induced decrease in neurogenesis in the hippocampus (38). DKI metrics of the clinical psychometric hepatic encephalopathy score (PHES) are correlated with the average AK and MK values in the lateral frontoorbital gyrus, caudate and thalamus rather than individual brain microstructures (39). Twelve non hippocampal regions discovered in our study, such as the left IFGoperc, right SFGmedial, right PHG, right FFG and left MTG, that are associated with cognitive changes after radiotherapy should be delineated as dose-avoidance ROIs for cognitive function protection. Alternatively, the brain RT field has gradually moved toward more personalized treatment for BM, with a trend of increased utility of SRS or stereotactic radiotherapy (SRT) and a decrease in WBRT (40). This allows better dose sparing to the normal brain and thus better protection to those functional areas (41). However, delineating those cognitive functional subregions is still necessary to further understand the dose/volume thresholds regardless of which brain RT techniques are used for treatment.

Note that our study has a few limitations. First, the sample size collected was relatively small considering the consistency of DKI parameters, which is due to the difficulty of data collection and patient compliance. However, the positive findings in our study warrant a larger sample size study to further confirm our hypothesis. In addition, most patients with brain tumors are older than 60 years and Junior high school, resulting in difficulties in patient compliance when asked to complete complex questionnaires. A longitudinal study with a longer follow-up is necessary to further explore the pathogenic mechanisms and neuroimaging features described here.

Conclusions

In conclusion, radiation brain injury can damage the

cognitive function of patients with brain metastases after brain radiotherapy. This cognitive impairment may be caused by the interaction of multiple microstructural indices and processes within different brain regions, not only the hippocampus. DTI and DKI can identify these microstructural changes early on. Future studies may solve the determination of threshold doses/volumes admissible for these regions. Understanding these brain substructures with a radiation dose limitation may lead to a new cognitive function protection model for radiotherapy in patients with of brain metastases.

Acknowledgments

The authors thank many respected professors and research units of the Department of Radiation Oncology, Sir Run Run Shaw Hospital, School of Medicine, Zhejiang University, and the Department of Radiation Oncology, Mayo Clinic Arizona and Research Center for Healthcare Data Science, Zhejiang Lab for helping in this study.
Funding: This work was supported by the Chinese National Natural Science Foundation (No. 81972849, to Xiaonan Sun); the National Key R&D Program of China (Nos. 2020AAA0109502 and 2019YFB1311800, to Hongjian He); Major Scientific Project of Zhejiang Lab (No. 2020ND8AD01, to Hongjian He); the China Postdoctoral Science Foundation (Nos. 2020TQ0296 and 2021M692961, to Qiqi Tong) and National Natural Science Foundation of China (No. 82102139, to Qiqi Tong).

Footnote

Reporting Checklist: The authors have completed the STROBE reporting checklist. Available at https://qims.amegroups.com/article/view/10.21037/qims-22-1376/rc

Conflicts of Interest: All authors have completed the ICMJE uniform disclosure form (available at https://qims.amegroups.com/article/view/10.21037/qims-22-1376/coif). QT reports grants from the China Postdoctoral Science Foundation (Nos. 2020TQ0296 and 2021M692961), grants from National Natural Science Foundation of China (No. 82102139), during the conduct of the study. HH reports grants from the National Key R&D Program of China (Nos. 2020AAA0109502 and 2019YFB1311800), a grant from Major Scientific Project of Zhejiang Lab (No. 2020ND8AD01), during the conduct of the study. XS reports a grant from Chinese National Natural Science Foundation (No. 81972849), during the conduct of the study. The other authors have no conflicts of interest to declare.

Ethical Statement: The authors are accountable for all aspects of the work in ensuring that questions related to the accuracy or integrity of any part of the work are appropriately investigated and resolved. The study was conducted in accordance with the Declaration of Helsinki (as revised in 2013). The study was approved by the ethics committee of Sir Run Run Shaw Hospital (No. 20200416001) and informed consent was taken from all individual participants.

References

1. Schouten LJ, Rutten J, Huveneers HA, Twijnstra A. Incidence of brain metastases in a cohort of patients with carcinoma of the breast, colon, kidney, and lung and melanoma. Cancer 2002;94:2698-705.
2. Murray KJ, Scott C, Greenberg HM, Emami B, Seider M, Vora NL, Olson C, Whitton A, Movsas B, Curran W. A randomized phase III study of accelerated hyperfractionation versus standard in patients with unresected brain metastases: a report of the Radiation Therapy Oncology Group (RTOG) 9104. Int J Radiat Oncol Biol Phys 1997;39:571-4.
3. Cochran DC, Chan MD, Aklilu M, Lovato JF, Alphonse NK, Bourland JD, Urbanic JJ, McMullen KP, Shaw EG, Tatter SB, Ellis TL. The effect of targeted agents on outcomes in patients with brain metastases from renal cell carcinoma treated with Gamma Knife surgery. J Neurosurg 2012;116:978-83.
4. Greene-Schloesser D, Robbins ME, Peiffer AM, Shaw EG, Wheeler KT, Chan MD. Radiation-induced brain injury: A review. Front Oncol 2012;2:73.
5. Ceresoli GL, Cappuzzo F, Gregorc V, Bartolini S, Crinò L, Villa E. Gefitinib in patients with brain metastases from non-small-cell lung cancer: a prospective trial. Ann Oncol

2004;15:1042-7.
6. Goldberg SB, Gettinger SN, Mahajan A, Chiang AC, Herbst RS, Sznol M, et al. Pembrolizumab for patients with melanoma or non-small-cell lung cancer and untreated brain metastases: early analysis of a non-randomised, open-label, phase 2 trial. Lancet Oncol 2016;17:976-83.
7. Greene-Schloesser D, Robbins ME. Radiation-induced cognitive impairment--from bench to bedside. Neuro Oncol 2012;14 Suppl 4:iv37-44.
8. Tringale KR, Nguyen TT, Karunamuni R, Seibert T, Huynh-Le MP, Connor M, Moiseenko V, Gorman MK, Marshall A, Tibbs MD, Farid N, Simpson D, Sanghvi P, McDonald CR, Hattangadi-Gluth JA. Quantitative Imaging Biomarkers of Damage to Critical Memory Regions Are Associated With Post-Radiation Therapy Memory Performance in Brain Tumor Patients. Int J Radiat Oncol Biol Phys 2019;105:773-83.
9. Tibbs MD, Huynh-Le MP, Karunamuni R, Reyes A, Macari AC, Tringale KR, Salans M, Yip A, Liu E, Simon A, McDonald CR, Hattangadi-Gluth JA. Microstructural Injury to Left-Sided Perisylvian White Matter Predicts Language Decline After Brain Radiation Therapy. Int J Radiat Oncol Biol Phys 2020;108:1218-28.
10. Qiu Y, Guo Z, Lin X, Li J, Li Z, Han L, Yang Y, Lv X. Standard radiotherapy for patients with nasopharyngeal carcinoma results in progressive tract-specific brain white matter alterations: A one-year follow-up via diffusion tensor imaging. Radiother Oncol 2021;159:255-64.
11. Brown PD, Gondi V, Pugh S, Tome WA, Wefel JS, Armstrong TS, et al. Hippocampal Avoidance During Whole-Brain Radiotherapy Plus Memantine for Patients With Brain Metastases: Phase III Trial NRG Oncology CC001. J Clin Oncol 2020;38:1019-29.
12. Gondi V, Pugh SL, Tome WA, Caine C, Corn B, Kanner A, Rowley H, Kundapur V, DeNittis A, Greenspoon JN, Konski AA, Bauman GS, Shah S, Shi W, Wendland M, Kachnic L, Mehta MP. Preservation of memory with conformal avoidance of the hippocampal neural stem-cell compartment during whole-brain radiotherapy for brain metastases (RTOG 0933): a phase II multi-institutional trial. J Clin Oncol 2014;32:3810-6.
13. Brown PD, Jaeckle K, Ballman KV, Farace E, Cerhan JH, Anderson SK, Carrero XW, Barker FG 2nd, Deming R, Burri SH, Ménard C, Chung C, Stieber VW, Pollock BE, Galanis E, Buckner JC, Asher AL. Effect of Radiosurgery Alone vs Radiosurgery With Whole Brain Radiation Therapy on Cognitive Function in Patients With 1 to 3 Brain Metastases: A Randomized Clinical Trial. JAMA 2016;316:401-9.
14. Boire A, Brastianos PK, Garzia L, Valiente M. Brain metastasis. Nat Rev Cancer 2020;20:4-11.
15. Li Z, Gong T, Lin Z, He H, Zhong J. Fast and Robust Diffusion Kurtosis Parametric Mapping Using a Three-dimensional Convolutional Neural Network. IEEE Access 2019;PP:1-.
16. Xiong WF, Qiu SJ, Wang HZ, Lv XF. 1H-MR spectroscopy and diffusion tensor imaging of normal-appearing temporal white matter in patients with nasopharyngeal carcinoma after irradiation: initial experience. J Magn Reson Imaging 2013;37:101-8.
17. Zhuo J, Xu S, Proctor JL, Mullins RJ, Simon JZ, Fiskum G, Gullapalli RP. Diffusion kurtosis as an in vivo imaging marker for reactive astrogliosis in traumatic brain injury. Neuroimage 2012;59:467-77.
18. Wu G, Luo SS, Balasubramanian PS, Dai GM, Li RR, Huang WY, Chen F. Early Stage Markers of Late Delayed Neurocognitive Decline Using Diffusion Kurtosis Imaging of Temporal Lobe in Nasopharyngeal Carcinoma Patients. J Cancer 2020;11:6168-77.
19. Glenn GR, Jensen JH, Helpern JA, Spampinato MV, Kuzniecky R, Keller SS, Bonilha L. Epilepsy-related cytoarchitectonic abnormalities along white matter pathways. J Neurol Neurosurg Psychiatry 2016;87:930-6.
20. Bigot F, Castanon E, Baldini C, Hollebecque A, Carmona A, Postel-Vinay S, Angevin E, Armand JP, Ribrag V, Aspeslagh S, Varga A, Bahleda R, Menis J, Gazzah A, Michot JM, Marabelle A, Soria JC, Massard C. Prospective validation of a prognostic score for patients in immunotherapy phase I trials: The Gustave Roussy Immune Score (GRIm-Score). Eur J Cancer 2017;84:212-8.
21. Hensel A, Angermeyer MC, Riedel-Heller SG. Measuring cognitive change in older adults: reliable change indices for the Mini-Mental State Examination. J Neurol Neurosurg Psychiatry 2007;78:1298-303.
22. Rolls ET, Huang CC, Lin CP, Feng J, Joliot M. Automated anatomical labelling atlas 3. Neuroimage 2020;206:116189.
23. Zhang F, Ning L, O'Donnell LJ, Pasternak O. MK-curve - Characterizing the relation between mean kurtosis and alterations in the diffusion MRI signal. Neuroimage 2019;196:68-80.
24. Veraart J, Sijbers J, Sunaert S, Leemans A, Jeurissen B. Weighted linear least squares estimation of diffusion MRI parameters: strengths, limitations, and pitfalls. Neuroimage 2013;81:335-46.

25. Rola R, Raber J, Rizk A, Otsuka S, VandenBerg SR, Morhardt DR, Fike JR. Radiation-induced impairment of hippocampal neurogenesis is associated with cognitive deficits in young mice. Exp Neurol 2004;188:316-30.
26. Armstrong CL, Shera DM, Lustig RA, Phillips PC. Phase measurement of cognitive impairment specific to radiotherapy. Int J Radiat Oncol Biol Phys 2012;83:e319-24.
27. Monje ML, Vogel H, Masek M, Ligon KL, Fisher PG, Palmer TD. Impaired human hippocampal neurogenesis after treatment for central nervous system malignancies. Ann Neurol 2007;62:515-20.
28. Zhao W, Diz DI, Robbins ME. Oxidative damage pathways in relation to normal tissue injury. Br J Radiol 2007;80 Spec No 1:S23-31.
29. Zhao W, Robbins ME. Inflammation and chronic oxidative stress in radiation-induced late normal tissue injury: therapeutic implications. Curr Med Chem 2009;16:130-43.
30. Belyk M, Brown S, Lim J, Kotz SA. Convergence of semantics and emotional expression within the IFG pars orbitalis. Neuroimage 2017;156:240-8.
31. Koshimori Y, Segura B, Christopher L, Lobaugh N, Duff-Canning S, Mizrahi R, Hamani C, Lang AE, Aminian K, Houle S, Strafella AP. Imaging changes associated with cognitive abnormalities in Parkinson's disease. Brain Struct Funct 2015;220:2249-61.
32. Acheson DJ, Hagoort P. Stimulating the brain's language network: syntactic ambiguity resolution after TMS to the inferior frontal gyrus and middle temporal gyrus. J Cogn Neurosci 2013;25:1664-77.
33. Matchin W, Hammerly C, Lau E. The role of the IFG and pSTS in syntactic prediction: Evidence from a parametric study of hierarchical structure in fMRI. Cortex 2017;88:106-23.
34. Siok WT, Niu Z, Jin Z, Perfetti CA, Tan LH. A structural-functional basis for dyslexia in the cortex of Chinese readers. Proc Natl Acad Sci U S A 2008;105:5561-6.
35. Hoffman P, Binney RJ, Lambon Ralph MA. Differing contributions of inferior prefrontal and anterior temporal cortex to concrete and abstract conceptual knowledge. Cortex 2015;63:250-66.
36. Peelen MV, Downing PE. Selectivity for the human body in the fusiform gyrus. J Neurophysiol 2005;93:603-8.
37. Peiffer AM, Leyrer CM, Greene-Schloesser DM, Shing E, Kearns WT, Hinson WH, Tatter SB, Ip EH, Rapp SR, Robbins ME, Shaw EG, Chan MD. Neuroanatomical target theory as a predictive model for radiation-induced cognitive decline. Neurology 2013;80:747-53.
38. Schindler MK, Forbes ME, Robbins ME, Riddle DR. Aging-dependent changes in the radiation response of the adult rat brain. Int J Radiat Oncol Biol Phys 2008;70:826-34.
39. Gupta P, Vyas S, Salan T, Jain C, Taneja S, Dhiman RK, Singh P, Ahuja CK, Ray N, Govind V. Whole brain atlas-based diffusion kurtosis imaging parameters for evaluation of minimal hepatic encephalopathy. Neuroradiol J 2022;35:67-76.
40. Mathis NJ, Wijetunga NA, Imber BS, Pike LRG, Yang JT. Recent Advances and Applications of Radiation Therapy for Brain Metastases. Curr Oncol Rep 2022;24:335-42.
41. Brown PD, Ballman KV, Cerhan JH, Anderson SK, Carrero XW, Whitton AC, Greenspoon J, Parney IF, Laack NNI, Ashman JB, Bahary JP, Hadjipanayis CG, Urbanic JJ, Barker FG 2nd, Farace E, Khuntia D, Giannini C, Buckner JC, Galanis E, Roberge D. Postoperative stereotactic radiosurgery compared with whole brain radiotherapy for resected metastatic brain disease (NCCTG N107C/CEC·3): a multicentre, randomised, controlled, phase 3 trial. Lancet Oncol 2017;18:1049-60.

Cite this article as: Xie X, Feng M, Rong Y, Hu J, Zhou W, Li Y, Liao H, Shi L, He H, Tong Q, Sun X. Whole brain atlas-based diffusion kurtosis imaging parameters for the evaluation of multiple cognitive-related brain microstructure injuries after radiotherapy in lung cancer patients with brain metastasis. Quant Imaging Med Surg 2023;13(8):5321-5332. doi: 10.21037/qims-22-1376

Supplementary

Table S1 Region of interest analysis of subacute WBRT effect on each DKI parameter: mean percentage change and P values by one-sample *t*-test

Region of interest	MD		FA		MK		AK	
	Percentage change	P value	Percentage change	P value	Percentage change	P value	Percentage change	P value
Left precentral gyrus	3.81 (11.07)	0.16	−4.06 (6.83)	0.04*	−2.55 (4.94)	0.05*	−2.50 (3.20)	0.01*
Left middle frontal gyrus	1.84 (5.1)	0.18	−0.71 (4.89)	0.54	−1.55 (2.54)	0.04*	−1.51 (2.67)	0.04*
Left opercular part of inferior frontal gyrus	1.48 (3.55)	0.12	−0.75 (6.37)	0.62	−1.36 (2.12)	0.02*	−1.58 (2.14)	0.02*
Left triangular part of inferior frontal gyrus	2.36 (4.09)	0.02*	−1.51 (3.76)	0.10	−1.67 (1.96)	0.004*	−2.16 (2.26)	0.004*
Left orbital part of inferior frontal gyrus	2.59 (5.72)	0.09	−1.38 (5.04)	0.26	−1.68 (2.63)	0.02*	−2.1 (2.87)	0.02*
Right orbital part of inferior frontal gyrus	4.66 (5.25)	0.004*	−2.47 (5.34)	0.06	−1.39 (2.78)	0.05*	−1.67 (2.5)	0.02*
Left rolandic operculum	2.33 (3.99)	0.02*	−0.55 (4.86)	0.639	−1.19 (1.81)	0.02*	−1.42 (1.7)	0.008*
Left olfactory cortex	7.27 (10.43)	0.03*	−1.42 (9.38)	0.52	−1.17 (3.55)	0.34	−1.25 (5.76)	0.48
Right medial orbital part of superior frontal gyrus	1.46 (6.01)	0.31	−1.87 (7.10)	0.37	−2.24 (3.13)	0.03*	−2.22 (3.18)	0.01*
Left insula	2.83 (5.12)	0.06	−0.3 (5.79)	0.82	−1.35 (2.19)	0.04*	−1.34 (1.97)	0.04*
Right middle cingulate & paracingulate gyri	2.93 (4.42)	0.01*	−3.1 (8.97)	0.15	−1.72 (2.42)	0.01*	−1.53 (1.96)	0.02*
Right parahippocampal gyrus	5.10 (9.65)	0.06	−1.63 (6.25)	0.28	−1.21 (1.86)	0.04*	−1.16 (2.96)	0.14
Left calcarine fissure and surrounding cortex	1.98 (4.75)	0.12	1.1 (5.25)	0.38	−1.41 (1.88)	0.01*	−1.2 (1.24)	0.004*
Right lingual gyrus	2.33 (6.05)	0.16	−0.59 (3.48)	0.48	−1.89 (1.76)	<0.001*	−1.19 (1.62)	0.01*
Left fusiform gyrus	2.38 (3.56)	0.04*	0.85 (6.6)	0.59	−1.55 (2.57)	0.04*	−1.63 (3.56)	0.08
Right fusiform gyrus	4.31 (7.04)	0.02*	0.29 (6.86)	0.86	−1.25 (1.58)	0.01*	−0.99 (3.54)	0.33
Left postcentral gyrus	2.82 (4.96)	0.02*	−1.81 (4.54)	0.108	−1.87 (2.34)	0.006*	−1.82 (1.58)	<0.001*
Left inferior parietal gyrus, excluding supramarginal and angular gyri	1.63 (4.14)	0.14	−0.76 (4.39)	0.47	−1.17 (1.6)	0.02*	−1.12 (1.88)	0.04*
Left supramarginal gyrus	1.58 (2.8)	0.02*	−1.05 (4.97)	0.381	−1.3 (1.74)	0.01*	−1.14 (1.88)	0.02*
Right angular gyrus	2.04 (6.2)	0.36	−1.49 (5.11)	0.233	−0.84 (2.73)	0.26	−0.99 (1.77)	0.04*
Left paracentral lobule	3.81 (11.07)	0.162	−4.06 (6.83)	0.04*	−2.55 (4.94)	0.05*	−2.5 (3.2)	0.01*
Right caudate nucleus	7.47 (9.21)	0.01*	−4.65 (14.94)	0.203	−3.69 (7.74)	0.06	−3.66 (5.56)	0.02*
Left superior temporal gyrus	1.62 (4.61)	0.20	−0.44 (5.8)	0.75	−1.23 (2.43)	0.08	−1.67 (2.05)	0.01*
Left temporal pole: superior temporal gyrus	0.23 (7.91)	0.902	-1.53 (9.15)	0.64	−1.09 (3.7)	0.44	−1.8 (2.63)	0.03*
Left middle temporal gyrus	2.57 (4.54)	0.04*	−1.08 (5.84)	0.58	−1.82 (1.99)	0.004*	−1.9 (2.05)	0.004*
Left temporal pole: middle temporal gyrus	3.06 (9.95)	0.26	−2.09 (11.89)	0.466	−1.92 (2.43)	0.01*	−2.55 (3.57)	0.01*
Left inferior temporal gyrus	2.41 (3.56)	0.01*	0.25 (6.09)	0.86	−1.78 (2.15)	0.006*	−2.12 (2.28)	0.004*
Right inferior temporal gyrus	2.61 (3.89)	0.04*	−0.15 (7.73)	>0.99	−1.63 (2.44)	0.04*	−1.5 (3.17)	0.12

*, P values indicate statistical significance (P≤0.05) after corrections for multiple comparisons. BM, brain metastasis; MMSE, Mini-Mental Status Examination; SD, standard deviation; MD, mean diffusivity; FA, fractional anisotropy; MK, mean kurtosis; AK, axial kurtosis.

https://dx.doi.org/10.21037/qims-22-1376